



HAL
open science

Pressure-dependent Raman scattering of polycrystalline KNb_{1-x}TaxO₃ solid solutions

Elizabeth Di Geronimo, Veronique Bornand, Philippe Baranek, Philippe
Papet

► **To cite this version:**

Elizabeth Di Geronimo, Veronique Bornand, Philippe Baranek, Philippe Papet. Pressure-dependent Raman scattering of polycrystalline KNb_{1-x}TaxO₃ solid solutions. SN Applied Sciences, 2020, 2 (11), pp.1882. 10.1007/s42452-020-03673-3 . hal-03360783v1

HAL Id: hal-03360783

<https://hal.science/hal-03360783v1>

Submitted on 29 Oct 2020 (v1), last revised 1 Oct 2021 (v2)

HAL is a multi-disciplinary open access archive for the deposit and dissemination of scientific research documents, whether they are published or not. The documents may come from teaching and research institutions in France or abroad, or from public or private research centers.

L'archive ouverte pluridisciplinaire **HAL**, est destinée au dépôt et à la diffusion de documents scientifiques de niveau recherche, publiés ou non, émanant des établissements d'enseignement et de recherche français ou étrangers, des laboratoires publics ou privés.

SN Applied Sciences

Pressure-dependent Raman scattering of polycrystalline KNb_{1-x}Ta_xO₃ solid solutions --Manuscript Draft--

| | |
|--|---|
| Manuscript Number: | SNAS-D-20-01178R2 |
| Full Title: | Pressure-dependent Raman scattering of polycrystalline KNb _{1-x} Ta _x O ₃ solid solutions |
| Article Type: | Research Article |
| Section/Category: | Materials Science |
| Funding Information: | |
| Abstract: | We report experimental and calculated Raman scattering investigations of KNb _{1-x} Ta _x O ₃ (x = 0.4, 0.5, 0.6) solid solutions as a function of hydrostatic pressure. The observed phase transitions sequence in the range from room pressure to 12 GPa is similar to the temperature-induced structural phase transformations: orthorhombic (ferroelectric) to tetragonal (ferroelectric) to cubic (paraelectric). Furthermore, it was observed that the domain of stability of ferroelectricity at high pressures increases with Nb-content. For the first time, some DFT calculations of theoretical Raman spectra are reported in order to support the experimental observations of pressure-induced phase transitions. |
| Keywords: | High pressure Raman spectroscopy; Phase transitions, Potassium niobate tantalate; DFT |
| Corresponding Author: | veronique bornand Institut Charles Gerhardt de Montpellier Montpellier, FRANCE |
| Corresponding Author Secondary Information: | |
| Corresponding Author's Institution: | Institut Charles Gerhardt de Montpellier |
| Corresponding Author's Secondary Institution: | |
| First Author: | Elizabeth Di Geronimo |
| First Author Secondary Information: | |
| Order of Authors: | Elizabeth Di Geronimo veronique bornand Philippe Baranek Philippe Papet |
| Order of Authors Secondary Information: | |
| Author Comments: | |
| Response to Reviewers: | last typo errors have been corrected |
| Suggested Reviewers: | Laurent Lebrun Pr, Institut National des Sciences Appliquees de Lyon laurent.lebrun@insa-lyon.fr Synthesis Characterization Modeling of ferroelectrics MS RAMACHANDRA RAO Pr, ITT Kharagpur msrrao@iitm.ac.in Electronic and magnetic oxides Vladimir Balitsky Head director, IEM RAS Chernogoloska balvlad@iem.as.ru Bulk oxide electronics |

| | |
|---|--|
| Order of Authors (with Contributor Roles): | Elizabeth Di Geronimo (Formal analysis: Equal; Investigation: Equal) |
| | veronique bornand (Conceptualization: Equal; Investigation: Equal; Methodology: Equal; Writing – original draft: Lead; Writing – review & editing: Lead) |
| | Philippe Baranek (Software: Lead; Writing – original draft: Equal; Writing – review & editing: Equal) |
| | Philippe Papet (Project administration: Lead; Supervision: Lead; Validation: Equal) |

[Click here to view linked References](#)

Pressure-dependent Raman scattering of polycrystalline $\text{KNb}_{1-x}\text{Ta}_x\text{O}_3$ solid solutions

E. Di Geronimo^{a,1}, V. Bornand^{a,2*}, Ph. Baranek^{b,3} and Ph. Papet^{a,4}

^a ICGM, Univ Montpellier, CNRS, ENSCM, Montpellier, France

^b EDF R&D, Department EFESE, EDF Lab Paris-Saclay, Palaiseau, France

¹ edigerod@gmail.com ORCID 0000-0002-7246-5304

² veronique.bornand@umontpellier.fr (corresponding author) ORCID 0000-0002-9656-2440

³ philippe.baranek@edf.fr ORCID 0000-0001-6305-2826

⁴ philippe.papet@umontpellier.fr ORCID 0000-0002-1227-3562

Abstract

We report experimental and calculated Raman scattering investigations of $\text{KNb}_{1-x}\text{Ta}_x\text{O}_3$ ($x = 0.4, 0.5, 0.6$) solid solutions as a function of hydrostatic pressure. The observed phase transitions sequence in the range from room pressure to 12 GPa is similar to the temperature-induced structural phase transformations: orthorhombic (ferroelectric) to tetragonal (ferroelectric) to cubic (paraelectric). Furthermore, it was observed that the domain of stability of ferroelectricity at high pressures increases with Nb-content. For the first time, some DFT calculations of theoretical Raman spectra are reported in order to support the experimental observations of pressure-induced phase transitions.

Keywords: high pressure Raman spectroscopy; phase transitions; potassium niobate tantalite; DFT

1. Introduction

Over the last decade, lead-free ferroelectrics have gained major interest in functional materials research. Among the large family of ferroelectrics, the perovskite-type solid solution $\text{KNb}_{1-x}\text{Ta}_x\text{O}_3$ (KNT) appears as a potential alternative for lead-based ceramics in a wide range of electromechanical device applications, due to its good piezoelectric properties as well as environmental issues and human health [1-4]. Solid solutions of KNT exist as a single phase for the whole range of compositions, and all the phases

1
2
3
4 crystallize in the perovskite structure but with different symmetries. Later studies have
5 focused mainly on investigating the crystallographic and domain structures of these
6 compounds. In an earlier work, Triebwasser established the composition-temperature
7 phase diagram for $\text{KNbO}_3\text{-KTaO}_3$, pointing out a rhombohedral-orthorhombic-tetragonal-
8 cubic phase sequence with increasing temperature [5]. Moreover, it has been reported that
9 in KNT-based ceramics like $(\text{K,Na})(\text{Ta,Nb})\text{O}_3$ and $(\text{K,Na,Li})(\text{Ta,Nb,Sb})\text{O}_3$ both the Curie
10 temperature (T_C) and orthorhombic-tetragonal phase transition temperature (T_{O-T}) shifted
11 to lower temperature as the concentration of Ta increases [6-9]. In addition, by using X-
12 ray absorption Huan *et al.* showed the contribution of Ta displacements along different
13 crystallographic orientations on $(\text{K,Na})\text{NbO}_3$ ceramics, which tends to enhance the
14 ferroelectric properties at the T_{O-T} [10]. Besides temperature variation, pressure change is
15 another important variable providing complementary information about the different
16 phase transitions that could be induced by pressure. Few reports deal with pressure-effect
17 in the KNT system, which essentially concerns KNbO_3 and Nb-rich solid solutions of
18 KNT. Gourdain *et al.* [11] and Kobayashi *et al.* [12] observed that the ferroelectric
19 orthorhombic phase is stable up to 8-10 GPa and transforms to the paraelectric cubic
20 phase through a weakly first-order transformation. Nevertheless, Shamim *et al.* [13]
21 reported an orthorhombic to tetragonal phase transition around 7 GPa. Shamim *et al.*
22 performed a high-pressure Raman study on KNT single crystals only for Nb-rich solid
23 solutions where an orthorhombic-tetragonal-cubic phase sequence was observed upon
24 pressure with a limited domain of stability of the tetragonal structure [14].

25
26
27
28
29
30
31
32
33
34
35
36
37
38
39
40
41
42
43 In the present paper, high-pressure Raman spectroscopy experiments have been
44 conducted on three polycrystalline samples, $\text{KNb}_{0.6}\text{Ta}_{0.4}\text{O}_3$ (KN60T40), $\text{KNb}_{0.5}\text{Ta}_{0.5}\text{O}_3$
45 (KN50T50) and $\text{KNb}_{0.4}\text{Ta}_{0.6}\text{O}_3$ (KN40T60) up to 12 GPa with the aim (1) to analyze the
46 pressure-dependent phase transitions of these compounds and (2) to investigate the effect
47 of Ta substitution on the possible sequences structural transitions of KNT polycrystalline
48 samples with pressure. Besides, some DFT calculations of theoretical Raman spectra are
49 reported in order to support the experimental observations of phase transition in the
50 Raman spectra. This is the first time that such a theoretical versus experimental Raman
51 study is conducted on KNT solid solutions.
52
53
54
55
56
57
58
59
60
61
62
63
64
65

2. Experimental procedure

KNb_{1-x}Ta_xO₃ (x = 0.4, 0.5, 0.6) powders were prepared by solid-state reaction of high purity K₂CO₃, Nb₂O₅ and Ta₂O₅ powders through a classical ceramic process. The starting raw materials were mixed stoichiometrically in ethanol and ground using an agate mortar and a pestle until a homogeneous dried mixture was obtained. In order to get a better reactivity, the mixed powders were uniaxial pressed and calcined at different temperature in a range 785 °C - 1150°C for 4h. After the calcination, the samples were ground and mixed with alumina balls in an automatic planetary grinding machine (Fritsch Pulverisette 6) for 30 minutes at 400 rpm. The mixed powders were then sieved through a 100µm. X-Ray Diffraction (XRD) using a PANAnalytical X'pert pro diffractometer with Cu-K_{α1} radiation was used to identify the crystalline structure of the studied samples. The data were collected over 20° to 100° 2θ range with a 0.016 step size. Profile matching was performed with the use of the software FULLPROF [15]. Raman experiments were carried out with a Horiba LabRAM aramis Raman spectrometer using a 488 nm line of Ar⁺ ion laser as the **exciting source**, which was focused on the surface of the sample by using an X 50 objective of a microscope. **Data below ~125cm⁻¹ are artefacts due to the Rayleigh filter cut-off.** Measurements were performed at room temperature both on increasing (up to 12 GPa) and decreasing pressure by using a membrane-type diamond anvil cell (DAC) with diamond culets of 500-µm diameter and a large angular access (50°) to collect the highest possible amount of scattered light. The sample was loaded along with a ruby sphere and a 4:1 methanol-ethanol mixture as the quasi-hydrostatic pressure-transmitting fluid into a chamber of 150 µm in diameter and 50 µm thick drilled in a stainless steel gasket. The DAC was closed by applying a pressure to the membrane, and the pressurization of the system was performed step-by-step using a homemade pressure controller equipped with a needle wire allowing a low helium flow rate to be delivered and a buffer system for low gas leak. The pressure was estimated based on the shift of the R₁ fluorescence line of the ruby [16, 17]. The Raman signal was obtained in the 100-1000 cm⁻¹ range after a 10 min acquisition time. No intensity normalization has been done on all the recorded spectra reported in this paper.

3. Results and discussions

Figure 1 shows the room temperature XRD patterns collected for the three investigated compositions. We obtained highly crystallized materials without any detected second phases. In good agreement with published works, the Ta-rich $\text{KNb}_{0.4}\text{Ta}_{0.6}\text{O}_3$ (KN40T60) solid solution has a tetragonal symmetry while the Nb-rich $\text{KNb}_{0.6}\text{Ta}_{0.4}\text{O}_3$ (KN60T40) solid solution has an orthorhombic symmetry [5,14,18]. As already reported on KNT systems [5,18], $\text{KNb}_{0.5}\text{Ta}_{0.5}\text{O}_3$ (KN50T50) is located at the limit between tetragonal and orthorhombic phases. However, in this work, best refinement could be obtained with an orthorhombic symmetry with this composition (Table 1). EDX analyses of each sample have confirmed the right stoichiometry of the powders, with no major compositional dispersion.

3.1. Hydrostatic pressure study

Room temperature Raman spectra of the KNT samples with increasing pressure are shown in Figure 2. We observe that the main features of the samples are modified as function of the pressure. This can give us a direct indication that structural phase transitions occurred in the materials within the investigated pressure range. Moreover, after releasing the high-pressure the powders recover their initial crystal structures, showing that changes are reversible without any relaxing or hysteresis phenomena.

Phase transitions in ABO_3 -type alkali metal tantalates and niobates can be understood in terms of soft optical phonons, which may primarily involve either the vibrations or the rotations of the oxygen octahedral. The phase transitions are attributed to the condensation of these soft modes [19]. As it was shown in the reference [20, and other experimental and theoretical works cited in], these soft phonon are mainly IR-active and not Raman active (depending on the considered phase) and always involve a displacement and a deformation of the oxygen octahedra while the roles of A and B cations vary among the materials and between high and low pressure phase transitions.

Raman studies on similar solid solutions of KNT depending on temperature have pointed out the main signatures of the different phase transitions induced by temperature, which

1
2
3
4 are mainly dominated by bands related to the internal modes of the (Nb,Ta)O₆ octahedra
5 [20-22]. The modes around 840 cm⁻¹, 560 cm⁻¹ and the resonance-depth at 200 cm⁻¹ will
6 be the main features in the analyses of pressure induced phase transitions for this
7 investigation. These Raman active modes are associated to the (Nb,Ta)O₆ octahedra with
8 O_h symmetry which correspond to the Nb-O bond, and the stretch and bend vibrations of
9 the O-Nb-O modes.
10

11
12
13
14
15
16
17 With increasing pressures and according to the composition, a series of orthorhombic to
18 tetragonal to cubic (Nb-rich solid solutions) or tetragonal to cubic (Ta-rich solid
19 solutions) phase transitions can be observed.
20

21
22 A decrease in the resonance-depth at 200 cm⁻¹ and the loss of the low-wavenumber wing
23 of the 560 cm⁻¹ mode due to a transformation of the B₁(TO₃) and B₂(TO₃) modes into
24 E(TO₃) are the main characteristics of an orthorhombic to tetragonal (O-T) phase
25 transition [17,18]. The spectral deconvolution for the 500-650 cm⁻¹ region of KN60T40
26 and KN50T50 are shown in figure 3, which illustrates the possible identification of the
27 orthorhombic-to-tetragonal phase transition in KN60T40 and KN50T50 through the
28 shoulder around 530cm⁻¹ (followed by the * symbol). Specifically, it can be clearly seen
29 how as the pressure increases the B₁(TO₃) mode disappears while the B₂(TO₃) modes
30 transforms into the E(TO₃) mode and the phase transition takes place. The phase
31 transformations might occur around 3 to 4 GPa for both KN60T40 and KN50T50
32 samples.
33

34
35
36
37
38
39
40
41
42 Three criteria can be followed to identify the tetragonal to cubic (T-C) phase transition
43 and its associated critical pressure range. With increasing wavenumbers, we can quote:
44 (1) the fading of the resonance depth around 200 cm⁻¹ until it almost vanishes [22], (2)
45 the appearance of a mode around 450 cm⁻¹ which is first-order Raman inactive and can be
46 only observed in second-order scattering spectra in the cubic phase [20,24], and (3) the
47 disappearance of the first-order A₁(LO₃) mode around 840 cm⁻¹ which is forbidden in the
48 cubic phase [20]. Qualitatively, the three compositions investigated in this study have the
49 same high-pressure Raman signatures suggesting similar high-pressure crystal symmetry.
50 The high-pressure spectra obtained in our investigation are similar to those reported by
51 Manlief *et al.* at high temperatures [20]. At Room temperature, this T-C transition is
52
53
54
55
56
57
58
59
60
61
62
63
64
65

1
2
3
4 located around 7-8 GPa for KN60T40 and KN50T50, and decreases around 5-6 GPa for
5
6 the KN40T60 sample. The persistence of broad spectral features, even though a general
7
8 loss in intensity can be observed along with a strong increase of the background signal, is
9
10 a direct evidence that the material is not strictly speaking cubic on a local level, a
11
12 behavior which is very commonly observed in ferroelectrics due to local polar
13
14 fluctuations and/or local composition changes [22,23,25]. Existence of first-order Raman
15
16 scattering in $Pm3m$ structure refers to as disorder-induced Raman scattering and can be
17
18 assigned to nanopolar domains, initiated from the fluctuations of the Nb and Ta ions
19
20 among its allowed positions, whose structure is locally different from the average one
21
22 [26,27].
23

24
25 The transition pressures for the studied compositions were assigned from the above
26
27 analysis and reviewed in Figure 4. High pressure Raman studies have been already
28
29 performed for KN60T40 crystals by Shamim *et al.* [14]. The authors reported that the O-
30
31 T and T-C phase transitions might be at around 3 and 4 GPa, respectively. However, in
32
33 our work, concerning polycrystalline materials, while the phase sequence is maintained,
34
35 the domain of stability of the tetragonal phase, and the ferroelectric region, seems to be
36
37 larger. In addition, we can observe that as we increase the amount of tantalum the T-C
38
39 transition pressure and the associated ferroelectric-paraelectric transition line decrease.
40
41 This may be due to the atomic substitution that can cause a similar effect to the pressure
42
43 [14], showing a connected chemical pressure and physical pressure effect.
44

45 **3.2. Interpretation of Raman spectra : insights from theory**

46 **3.2.1. Theoretical determination of the Raman spectra**

47
48 The theoretical Raman spectra were calculated by using the Density Functional Theory
49
50 (DFT) (at 0° K). The theoretical data were obtained with the periodic CRYSTAL14 [30,
51
52 31]. The used exchange – correlation functional is the hybrid PBE0 functional [32] which
53
54 was shown to be the most adequate for the accurate description of the structural,
55
56 electronic, vibrational and dielectric properties in agreement with experimental data for
57
58 this family of materials [33]. Regarding the basis sets, an all – electron Gaussian type
59
60 basis set was used for O; K, Nb and Ta were described with Gaussian type basis sets
61
62
63
64
65

1
2
3
4 combined with pseudopotentials. A full description of these basis sets is given in
5 reference [34]. As regards the computational conditions for the evaluation of the
6 Coulomb and exchange series, the adopted thresholds on the overlap as defined in the
7 CRYSTAL manual [31] are 10^{-8} , 10^{-8} , 10^{-8} , 10^{-8} and 10^{-16} a.u.. Calculations were
8 performed with a $8 \times 8 \times 8$ Monkhorst – Pack k -point mesh [35]. The Γ -point harmonic
9 frequencies were calculated in the frozen phonons approximation.

10
11
12
13
14
15 The computed spectra were calculated considering ideal powders, with no preferred
16 orientation, and assuming an incident light with a wavelength of 488 nm. They were
17 convoluted with a Gaussian equation with a damping factor of 8cm^{-1} .

18
19
20
21
22
23 The different crystals have been simulated via a supercell approach. A $2 \times 2 \times 2$ supercell
24 of the primitive $\text{K}(\text{Nb},\text{Ta})\text{O}_3$ have been used ; for each “commensurate” concentration, all
25 non-identical substitution patterns have been considered. For each of them, the lattice
26 parameters and internal coordinates have been optimized, maintaining the cubic Pm-3m
27 symmetry (10 configurations by concentration). For the configuration minimizing the
28 total energy, the calculation of Γ phonons was performed in order to determine the
29 unstable mode leading to the tetragonal or orthorhombic phases of $\text{KNb}_{1-x}\text{Ta}_x\text{O}_3$. For
30 each concentration, the most stable configuration was retained and its equation of state
31 was determined by fitting the calculated total energy E versus volume V curves by an
32 integrated Murnaghan function. The volume $V(P)$ is deduced from $E(V)$. For each
33 volume, E is minimized with respect to the crystallographic parameters : there are 8, 2
34 and 60 parameters to be optimized for the cubic, tetra and orthorhombic phases,
35 respectively. Table 1 summarizes the obtained lattice parameters both theoretically and
36 experimentally in this work : the average error between the theoretical and experimental
37 results is about 0.5 %. These simple models have been used to determine the different
38 Raman spectra described in this paper.

3.2.2. Theoretical and experimental spectra

39
40
41
42
43
44
45
46
47
48
49
50
51
52
53
54
55
56
57
58
59
60
61
62
63
64
65
Figure 5 shows the experimental spectra compared with the computed ones at room
pressure and room temperature for the different $\text{KNb}_{1-x}\text{Ta}_x\text{O}_3$ ($x=0.6, 0.5, 0.4$) solid
solutions. The calculations were performed in (1) a harmonic approximation and (2) at 0°

1
2
3
4 K while the KTN system is (1) highly anharmonic and (2) the experiments were
5 performed at room temperature. Besides, disorder in the system and possible local
6 fluctuations in Nb and Ta ionic positions are responsible for the wide bands obtained in
7 experiments while background subtraction could not be done. Then a discrepancy
8 between the experimental and theoretical calculations will arise.
9

10 The experimental and computed spectra at room temperature and different pressures
11 (3GPa, 7GPa and 10GPa) for the investigated solid solutions are displayed in figures 6 to
12 8. For each pressure and each composition different spectra were calculated before being
13 compared to experimental data. Discrepancies and/or shifts between calculated and
14 observed spectra still subsist while the pressure is increased, attributed to the
15 approximation required in the computation algorithm. However, comparison between
16 theoretical values and available experimental ones are in a decent agreement specifically
17 when the transition from the tetragonal to the cubic phase takes place. Globally, DFT
18 studies confirm (1) the pressure-induced phase-transition sequences observed for each
19 system and (2) the pressure ranges in which phase transformations occur. The Ta-rich
20 $\text{KNb}_{0.4}\text{Ta}_{0.6}\text{O}_3$ solid solution undergoes a tetragonal to cubic phase transition below
21 3GPa. On the other side, the Nb-rich $\text{KNb}_{0.6}\text{Ta}_{0.4}\text{O}_3$ solid solution starts an orthorhombic
22 to tetragonal phase transition around 3GPa while the tetragonal to cubic phase transition
23 is already complete at 7GPa. The $\text{KNb}_{0.5}\text{Ta}_{0.5}\text{O}_3$ solid, located at the orthorhombic –
24 tetragonal boundary at room pressure, begins a total orthorhombic to tetragonal
25 transformation around 3 GPa while above 7 GPa the system is already cubic.
26
27
28
29
30
31
32
33
34
35
36
37
38
39
40
41
42
43

44 **4. Conclusion**

45 We have conducted pressure-dependent Raman scattering experiments of $\text{KNb}_{1-x}\text{Ta}_x\text{O}_3$ (x
46 = 0.4, 0.5, 0.6) polycrystalline samples, which provide evidence of pressure induce phase
47 transitions. The phase transition sequences obtained in this work are similar to the
48 temperature-dependent structural transformations reported in the literature. In addition,
49 the tetragonal to cubic phase transition occurs at higher pressures than the values reported
50 for mixed crystals of the sample composition. This could suggest an enhancement of the
51 ferroelectricity in polycrystalline solid solutions. Moreover, the domain of stability of
52 ferroelectricity at high pressures decreases as the amount of tantalum increases.
53
54
55
56
57
58
59
60
61
62
63
64
65

1
2
3
4
5
6 **Acknowledgements**

7 The authors wish to thank L. Daenens and J. Haines for their technical help in performing
8 pressure-induced Raman-scattering experiments.
9

10
11
12
13 The authors declare that they have no known competing financial interests or personal
14 relationships that could have appeared to influence the work reported in this paper.
15
16
17

18
19 **References**

- 20 [1] Cross LE (2004) Materials science - Lead-free at last, Nature 432:24-25.
21
22 [2] Rodel J, Klaus WJ, Seifert TP, Anton EM, Granzow T (2009) Perspective on the
23 development of lead-free piezoceramics, J. Am. Ceram. Soc. 92:1153-1177.
24
25 [3] Eichel RA, Kungl H (2010) Recent developments and future perspectives of lead-free
26 ferroelectrics, Funct. Mat. Lett. 3:1-4.
27
28 [4] Panda PK, Sahoo S (2015) PZT to lead-free ceramics: a review, Ferroelectrics
29 474:128-143.
30
31 [5] Triebwasser S (1959) Study of ferroelectric transitions of solid solutions single
32 crystals of $\text{KNbO}_3\text{-KTaO}_3$, Phys. Rev. 114:63-70.
33
34 [6] Schiemer J, Liu Y, Carpenter M, Withers R (2012) The Effect of Ta Doping on the
35 Phase Transitions and the Piezoelectric and Ferroelectric Properties of $\text{K}_{0.35}\text{Na}_{0.65}\text{NbO}_3$,
36 Ferroelectrics 429:95-102.
37
38 [7] Lv Y, Wang C, Zhang J, Wu L, Zhao M, Xu J (2009) Tantalum influence on physical
39 properties of $(\text{K}_{0.5}\text{Na}_{0.5})(\text{Nb}_{1-x}\text{Ta}_x)\text{O}_3$ ceramics, Mater. Res. Bull. 44:284-287.
40
41 [8] Chang Y, Yang ZP, Ma D, Liu Z, Wang Z (2008) Phase transitional behavior,
42 microstructure, and electrical properties in Ta-modified $[(\text{K}_{0.458}\text{Na}_{0.542})_{0.96}\text{Li}_{0.04}]\text{NbO}_3$
43 lead-free piezoelectric ceramics, J. Appl. Phys. 104:024109.
44
45 [9] Yang Z, Chang Y, Wei L (2007) Phase transitional behavior and electrical properties
46 of lead-free $(\text{K}_{0.44}\text{Na}_{0.52}\text{Li}_{0.04})(\text{Nb}_{0.96-x}\text{Ta}_x\text{Sb}_{0.04})\text{O}_3$ piezoelectric ceramics, Appl. Phys.
47 Lett. 90:042911
48
49
50
51
52
53
54
55
56
57
58
59
60
61
62
63
64
65

- 1
2
3
4 [10] Huan Y, Wang X, Li L (2014) Displacement of Ta-O bonds near polymorphic phase
5 transition in Li-Ta-Sb-modified (K, Na)NbO₃ ceramics, Appl. Phys. Lett. 104:242905.
6
7 [11] Gourdain D, Moya E, Chervin JC, Canny B, Pruzan Ph (1995) Ferroelectric-
8 paraelectric phase transition in KNbO₃ at high pressure, Phys. Rev. B 52:3108-3112.
9
10 [12] Kobayashi Y, Endo S, Ashida T, Ming LC, Kikegawa (2000) T, High-pressure phase
11 above 40 GPa in ferroelectric KNbO₃, Phys. Rev. B 61:5819-5822.
12
13 [13] Shamim MMd, Ishidate T (2000) Anomalous mode coupling and phase transition of
14 KNbO₃ under high pressure, Solid State Comm. 113:713-717.
15
16 [14] Shamim MMd, Ishidate T, Ohi K (2003) High pressure Raman study of KNbO₃-
17 KTaO₃ and KNbO₃-NaNbO₃ mixed crystals, J. Phys. Soc. Jpn 72 :551-555.
18
19 [15] Rodriguez-Carvajal J (2005) FullProf.
20 <https://www.ill.eu/sites/fullprof/php/downloads.html>. Accessed 2008.
21
22 [16] Mao H, Xu J, Bell P (1986), Calibration of the ruby pressure gauge to 800KBar
23 under quasi-hydrostatic conditions, J. Geophysical Res. 91:4673-4676.
24
25 [17] Sherman WF, Wilkinson GR (1980) Raman and infrared studies of crystals at
26 variable pressure and temperature. In: Clark RJH, Hester RE (eds) Advances in Infrared
27 and Raman Spectroscopy, Heyden, London, pp 158-336.
28
29 [18] Rytz D, Scheel HJ (1982) Crystal growth of KTa_{1-x}Nb_xO₃ (0<x<0.04) solid solutions
30 by a slow cooling method, J. Cryst. Growth 59:468-484.
31
32 [19] Fontana MD, Kugel GE, Vamvakas J, Carabatos C (1983) Persistence of tetragonal
33 Raman lines in cubic KNbO₃, Solid State Comm. 45:873-875.
34
35 [20] Manlief SK, Fan HY (1972) Raman spectrum of KTa_{0.64}Nb_{0.36}O₃, Phys. Rev. B
36 5:4046-4060.
37
38 [21] Zhang NN, Wei RS, Wang JY, Hu XB, Zhang HJ, Santos CC, Guedes I (2012)
39 Phase transition investigation by Raman spectroscopy in highly diluted KTN crystals, J.
40 Alloys Compd. 531:14-17.
41
42 [22] Bartasyte A, Kreisel J, Peng W, Guilloux-Viry M (2010) Temperature-dependent
43 Raman scattering of KTa_{1-x}Nb_xO₃ thin films, Appl. Phys. Lett. 96:262903.
44
45 [23] Pruzan Ph, Gourdain D, Chervin JC (2007) Vibrational dynamics and phase diagram
46 of KNbO₃ up to 30 GPa and from 20 to similar to 500K, Phase Transitions 80:1103-1130.
47
48
49
50
51
52
53
54
55
56
57
58
59
60
61
62
63
64
65

- 1
2
3
4 [24] Rahaman MM, Imai T, Miyazu T, Kobayashi J, Tsukada S, Helal MA (2014),
5 Relaxor-like dynamics of ferroelectric $K(\text{Ta}_{1-x}\text{Nb}_x)\text{O}_3$ crystals probed by inelastic light
6 scattering, *J. Appl. Phys.* 116:074110.
7
8
9 [25] Uwe H, Carter KB, Carter HL, Fleury PA (1986) Ferroelectric microregions and
10 Raman scattering in KTaO_3 , *Phys. Rev. B* 33:6436-6440.
11
12 [26] Sood AK, Chandrabbas N, Muthu DVS, Jayaraman A (1995) Phonon interference in
13 BaTiO_3 : High-pressure Raman study, *Phys. Rev. B* 51:8892-8896.
14
15 [27] Venkateswaran UD, Naik VM, Naik R (1998) High-pressure Raman studies of
16 polycrystalline BaTiO_3 , *Phys. Rev. B* 58:14256-14260.
17
18 [28] Shen Z, Hu ZP, Chong TC, Kuok MH (1995) Pressure-induced strong mode
19 coupling and phase transitions in KNbO_3 , *Phys. Rev. B.* 52:3976-3980.
20
21 [29] Li S, Ahuja R, Johansson B (2002) Pressure-induced phase transitions of KNbO_3 , *J.*
22 *Phys. Condens. Matter* 14:10873-10877.
23
24 [30] Dovesi R, Orlando R, Erba A, Zicovich-Wilson CM, Civalleri B, Casassa S,
25 Maschio L, Ferrabone M, De La Pierre M, D'Arco P, Noel Y, Causa M, Rerat M,
26 Kirtman B (2014) CRYSTAL14: a program for the Ab Initio investigation of crystalline
27 solids, *Int. J. Quantum Chem.* 114:1287-1317.
28
29 [31] Dovesi R, Saunders VR, Roetti C, Orlando R, Zicovich-Wilson CM, Pascale F,
30 Civalleri B, Doll K, Harrison NM, Bush IJ, D'Arco P, Llunell M, Causà M, Noël Y
31 (2014) CRYSTAL14 User's Manual (University of Torino, Torino, 2014).
32
33 [32] Adamo C, Barone V (1999) Toward reliable density functional methods without
34 adjustable parameters: The PBE0 model, *J. Chem. Phys.* 110:6158-6170.
35
36 [33] Sophia G, Baranek Ph, Sarrazin C, Rérat M, Dovesi R (2013) First-principles study
37 of the mechanisms of the pressure-induced dielectric anomalies in ferroelectric
38 perovskites, *Phase Transitions* 86:068-1084.
39
40 [34] Web site: <http://www.crystal.unito.it/basis-sets.php>
41
42 [35] Monkhorst H, Pack J (1976) Special points for Brillouin zone integrations, *Phys.*
43 *Rev. B.* 13:5188-5192.
44
45
46
47
48
49
50
51
52
53
54
55
56
57
58
59
60
61
62
63
64
65

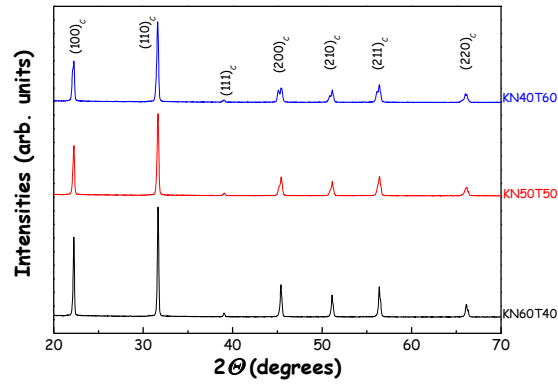


Figure 1. X-ray diffraction patterns of KNb_{1-x}Ta_xO₃ polycrystalline samples in the perovskite phase.

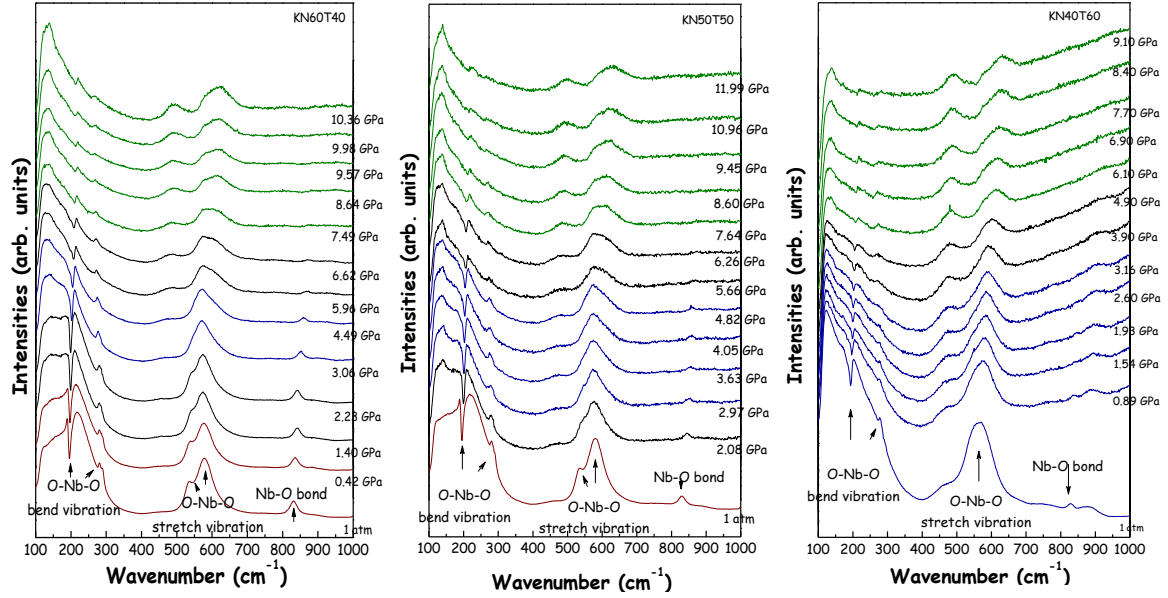


Figure 2. Raman spectra at room temperature of three different polycrystalline samples of $\text{KNb}_{1-x}\text{Ta}_x\text{O}_3$ as function of pressure. Colors are guide lines for the reader : brown spectra (orthorhombic phase), blue spectra (tetragonal phase), green spectra (cubic phase), black spectra (phase transition areas).

1
2
3
4
5
6
7
8
9
10
11
12
13
14
15
16
17
18
19
20
21
22
23
24
25
26
27
28
29
30
31
32
33
34
35
36
37
38
39
40
41
42
43
44
45
46
47
48
49
50
51
52
53
54
55
56
57
58
59
60
61
62
63
64
65

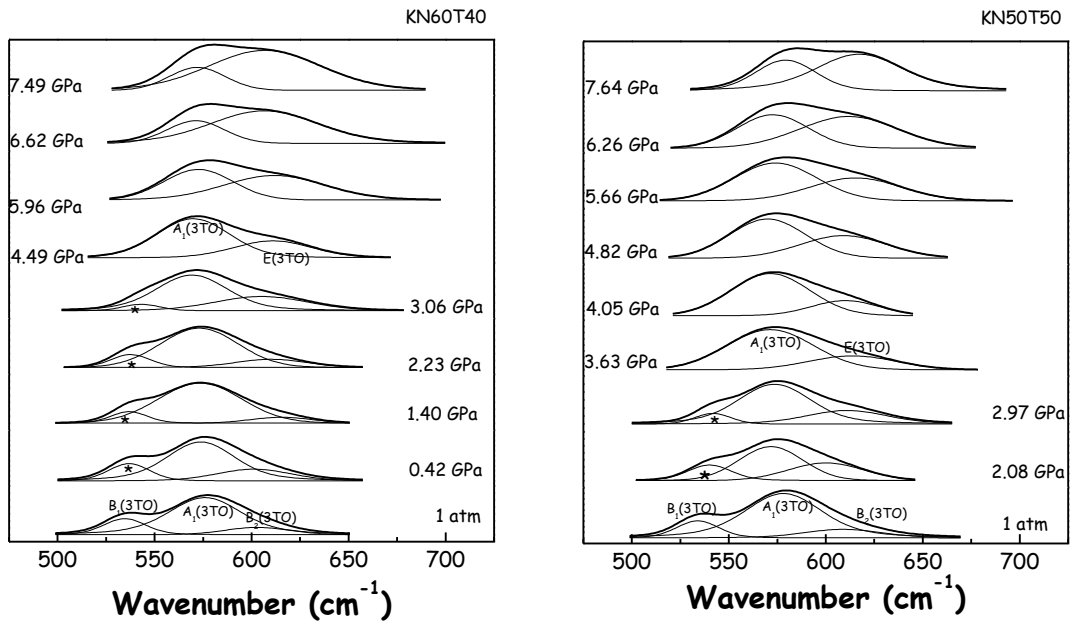


Figure 3. Raman spectra for $\text{KNb}_{1-x}\text{Ta}_x\text{O}_3$ ($x=0.4, 0.5$) in the $500\text{-}650\text{ cm}^{-1}$ region for polycrystalline samples as a function of increasing pressure. The spectral deconvolution illustrates the possible identification of the pressure-induced phase transitions that occur in the materials depending on the composition. (* follows the pressure-induced decrease of the $B_1(3TO)$ mode characteristic of the orthorhombic phase)

1
2
3
4
5
6
7
8
9
10
11
12
13
14
15
16
17
18
19
20
21
22
23
24
25
26
27
28
29
30
31
32
33
34
35
36
37
38
39
40
41
42
43
44
45
46
47
48
49
50
51
52
53
54
55
56
57
58
59
60
61
62
63
64
65

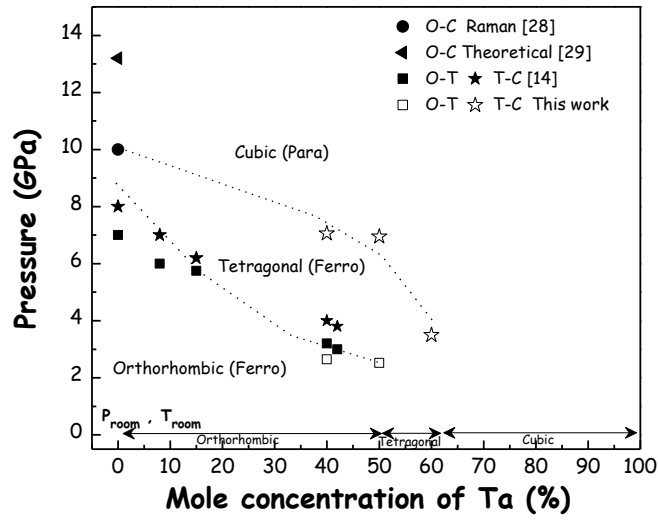


Figure 4. Summary of the pressure-composition phase diagram for $\text{KNb}_{1-x}\text{Ta}_x\text{O}_3$ from this work and literature. Dash lines are guides to the eyes for the points of this work.

1
2
3
4
5
6
7
8
9
10
11
12
13
14
15
16
17
18
19
20
21
22
23
24
25
26
27
28
29
30
31
32
33
34
35
36
37
38
39
40
41
42
43
44
45
46
47
48
49
50
51
52
53
54
55
56
57
58
59
60
61
62
63
64
65

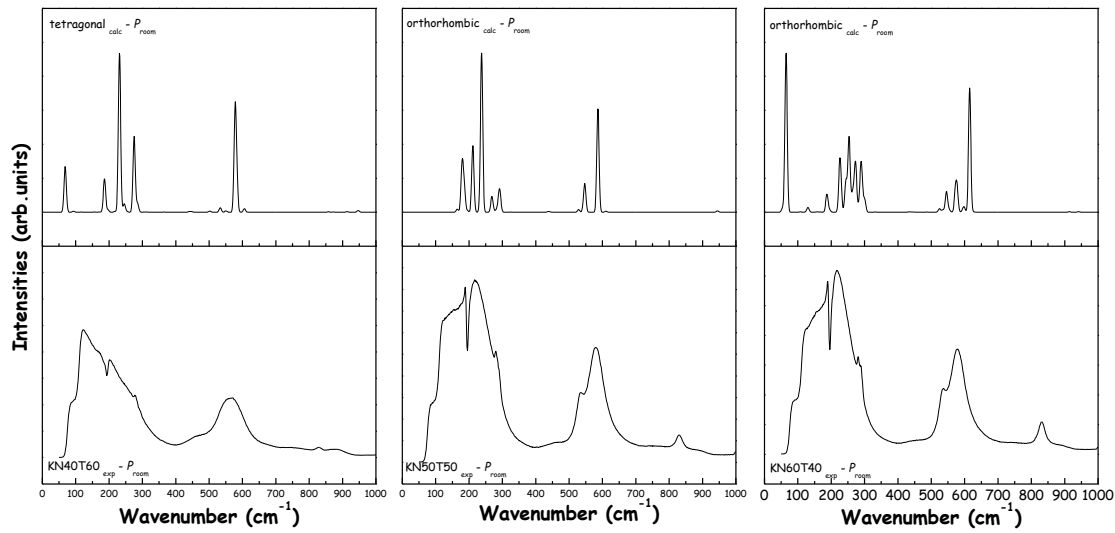


Figure 5. Calculated (up) and experimental (down) Raman spectra for KNb_{1-x}Ta_xO₃ (x=0.6, 0.5 and 0.4 from left to right) at room pressure.

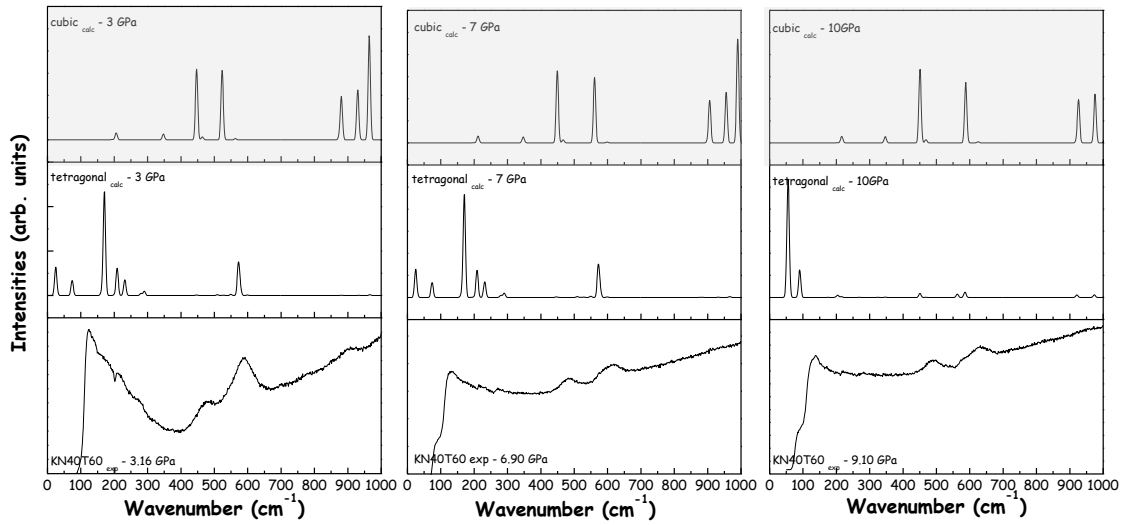


Figure 6. Calculated and experimental Raman spectra for $\text{KNb}_{0.4}\text{Ta}_{0.6}\text{O}_3$ at 3 GPa, 7 GPa and 10 GPa (from left to right). For each pressure, theoretical spectra were calculated with tetragonal and cubic symmetries. Grey area corresponds to the best agreement between DFT calculations and theoretical datas.

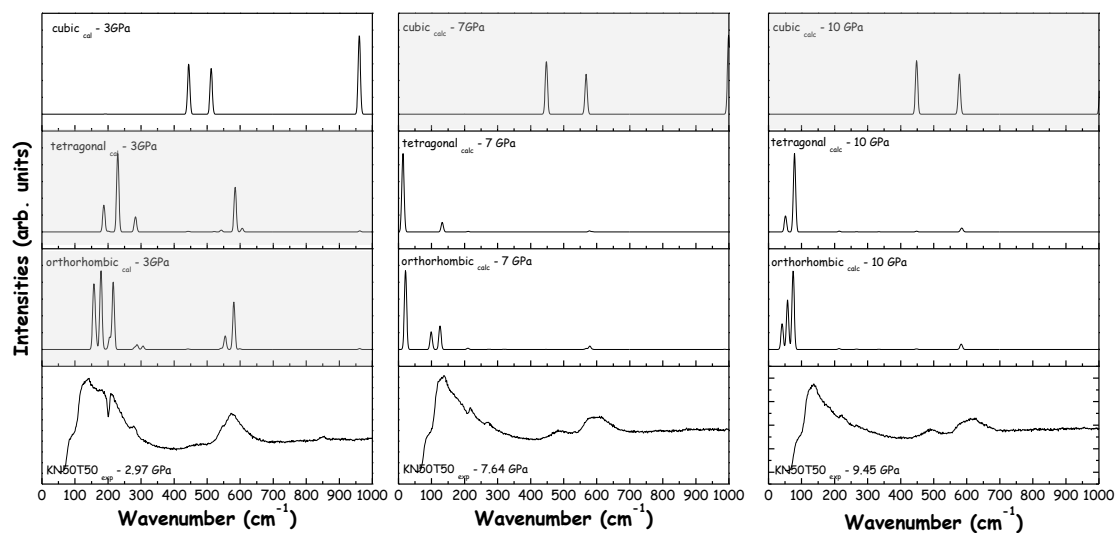


Figure 7. Calculated and experimental Raman spectra for $\text{KNb}_{0.5}\text{Ta}_{0.5}\text{O}_3$ at 3 GPa, 7 GPa and 10 GPa (from left to right). Grey area: best agreement. For each pressure, theoretical spectra were calculated with orthorhombic, tetragonal and cubic symmetries. Grey area corresponds to the best agreement between DFT calculations and theoretical datas

1
2
3
4
5
6
7
8
9
10
11
12
13
14
15
16
17
18
19
20
21
22
23
24
25
26
27
28
29
30
31
32
33
34
35
36
37
38
39
40
41
42
43
44
45
46
47
48
49
50
51
52
53
54
55
56
57
58
59
60
61
62
63
64
65

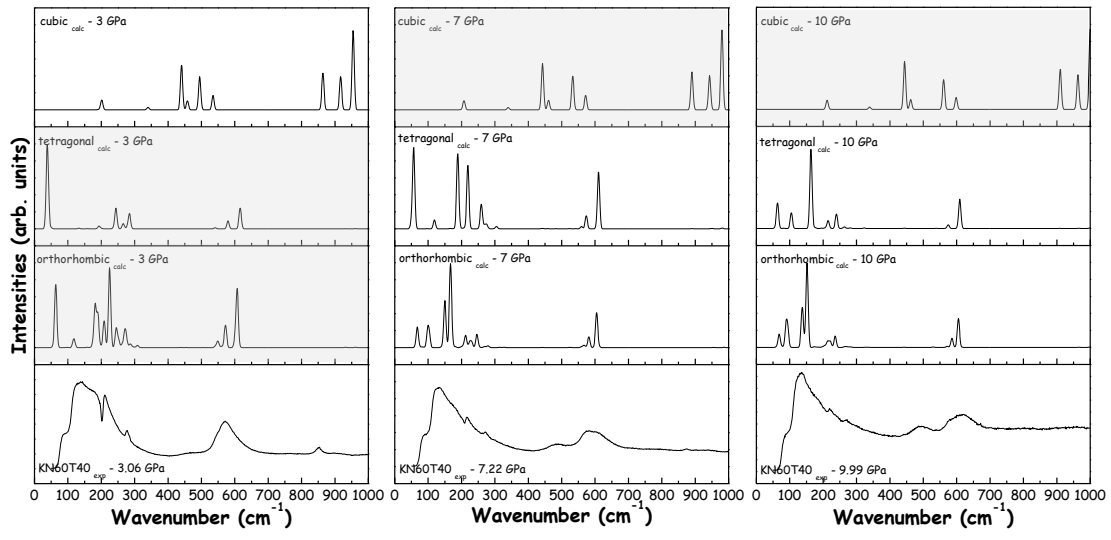


Figure 8. Calculated and experimental Raman spectra for $\text{KNb}_{0.6}\text{Ta}_{0.4}\text{O}_3$ at 3 GPa, 7 GPa and 10 GPa (from left to right). For each pressure, theoretical spectra were calculated with orthorhombic, tetragonal and cubic symmetries. Grey area corresponds to the best agreement between DFT calculations and theoretical datas

Table 1. Details of lattice parameters and cell volume obtained from the XRD patterns through a Le Bail analysis compared with the ones obtained theoretically in this work.

| Composition | Space Group | | a (Å) | b (Å) | c (Å) | V (Å ³) |
|---|-------------|-------|---------|---------|---------|-----------------------|
| KNb _{0.4} Ta _{0.6} O ₃ | <i>P4mm</i> | Exp. | 3.993 | 3.993 | 4.002 | 63.808 |
| | | Calc. | 3.985 | 3.985 | 4.076 | 64.727 |
| KNb _{0.5} Ta _{0.5} O ₃ | <i>Amm2</i> | Exp. | 3.992 | 5.649 | 5.702 | 64.292 |
| | | Calc. | 3.982 | 5.680 | 5.692 | 64.370 |
| KNb _{0.6} Ta _{0.4} O ₃ | <i>Amm2</i> | Exp. | 3.991 | 5.655 | 5.689 | 64.198 |
| | | Calc. | 3.982 | 5.663 | 5.674 | 63.974 |